Microtubule organization by kinesin motors and microtubule crosslinking protein MAP65

2013 J. Phys.: Condens. Matter 25 374103

(http://iopscience.iop.org/0953-8984/25/37/374103)

IOP PUBLISHING JOURNAL OF PHYSICS: CONDENSED MATTER
J. Phys.: Condens. Matter **25** (2013) 374103 (12pp) doi:10.1088/0953-8984/25/37/374103

Microtubule organization by kinesin motors and microtubule crosslinking protein MAP65

Joshua Pringle[1], Amutha Muthukumar[1,2], Amanda Tan[1], Laura Crankshaw[3], Leslie Conway[4] and Jennifer L Ross[1]

[1] Department of Physics, University of Massachusetts Amherst, Amherst, MA, USA
[2] Amherst Regional High School, Amherst, MA, USA
[3] St George's University School of Medicine, Grenada, West Indies
[4] Molecular and Cellular Biology Program, University of Massachusetts Amherst, Amherst, MA, USA

E-mail: rossj@physics.umass.edu

Received 30 January 2013, in final form 21 March 2013
Published 15 August 2013
Online at stacks.iop.org/JPhysCM/25/374103

Abstract
Microtubules are rigid, proteinaceous filaments required to organize and rearrange the interior of cells. They organize space by two mechanisms, including acting as the tracks for long-distance cargo transporters, such as kinesin-1, and by forming a network that supports the shape of the cell. The microtubule network is composed of microtubules and a bevy of associated proteins and enzymes that self-organize using non-equilibrium dynamic processes. In order to address the effects of self-organization of microtubules, we have utilized the filament-gliding assay with kinesin-1 motors driving microtubule motion. To further enhance the complexity of the system and determine if new patterns are formed, we added the microtubule crosslinking protein MAP65-1. MAP65-1 is a microtubule-associated protein from plants that crosslinks antiparallel microtubules, similar to mammalian PRC1 and fission yeast Ase1. We find that MAP65 can slow and halt the velocity of microtubules in gliding assays, but when pre-formed microtubule bundles are added to gliding assays, kinesin-1 motors can pull apart the bundles and reconstitute cell-like protrusions.

S Online supplementary data available from stacks.iop.org/JPhysCM/25/374103/mmedia

(Some figures may appear in colour only in the online journal)

1. Introduction

We seek to understand how nanoscale subunits can create 10–100 μm-scale structures utilizing non-equilibrium self-organization. Such self-organization has proven to be a powerful method for nanoscale and hierarchical organization harnessed by scientists and engineers interested in engineering adaptive materials. The cytoskeleton is a perfect material system to study non-equilibrium self-organization because it is an active mechano–chemical network that utilizes passive and active crosslinkers to restructure itself and the cell interior. Active crosslinkers are often motile enzymes, or motor proteins, that use the energy stored in nucleotide triphosphates to create motion and force. Motor proteins often work as collective groups. For instance, in muscles, many myosin II motors coordinate to cause large-scale muscle contraction. In the kidneys and intestines, axonemal dynein motors work in tandem to wave cilia causing fluid flow. Inside cells, teams of kinesins, cytoplasmic dyneins, and myosins walk intracellular cargos around using the microtubules and actin filaments as tracks. Similar teams of motors create, rearrange, and disassemble the mitotic spindle during cell division. In each of these instances, the motors and cytoskeletal filaments have a specific organization to enable the collective motors to perform their function. Further, this organization is created by motors and other associated proteins. Thus, understanding the ability of many motors to organize and rearrange filamentous

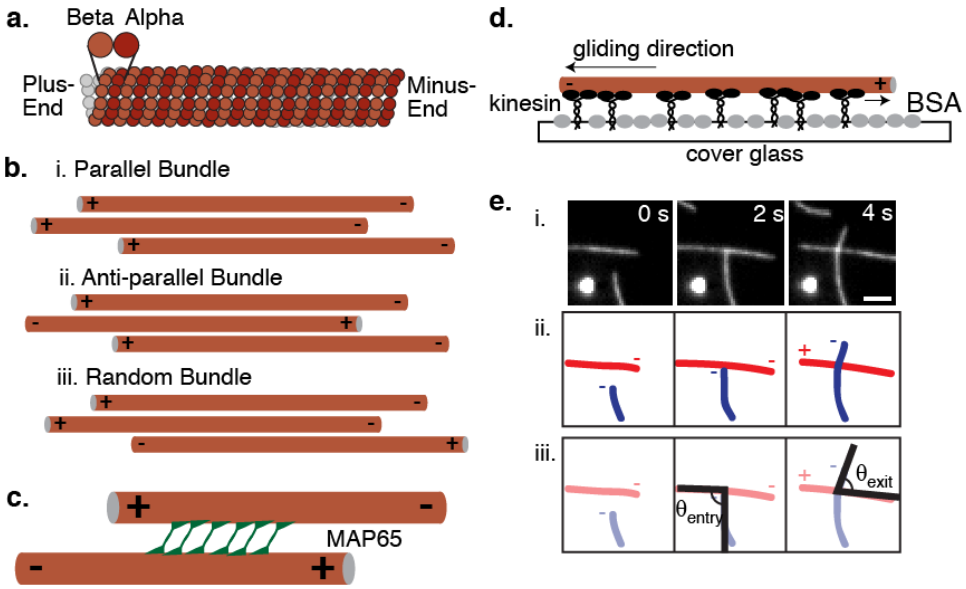

Figure 1. Types of microtubule bundles. (a) Microtubules are filaments made of a lattice of alpha–beta tubulin dimers. Dimers bind head to tail such that the structure is polarized. The end with the beta tubulin is called the plus-end. The end with the alpha tubulin is the minus-end. (b) Microtubules in cells are often bundled. Bundles can be (i) parallel all oriented the same way, (ii) antiparallel with plus-ends and minus-ends alternating, or (iii) random orientation. (c) MAP65 bundles microtubules antiparallel by binding periodically along the microtubule and projecting from the side of the microtubule at a 55°–65°angle when measured from the plus-end of the microtubule. (d) Schematic of the experimental method for microtubule filament gliding. The kinesin motors are adhered to the cover glass. The surface is blocked by BSA before microtubules are added. Kinesin motors walk toward the plus-end and propel the microtubule with the minus-end forward. (e) Example demonstrating an encounter between two microtubules and how the angles of entry and exit are measured. (i) Time series of three frames from a gliding assay where two microtubules encounter each other. Scale bar is 3 μm. (ii) Diagram of the same three frames with the microtubules traced. The minus-end is labeled at the leading end and the plus-end is the trailing end. (iii) Same schematic with the angle of entry (θ_{entry}) and angle of exit (θ_{exit}) labeled on the schematic.

networks is an important biological question with implications for non-equilibrium condensed matter.

There are three overlapping cytoskeletal networks in cells that utilize three different types of filaments: actin filaments, intermediate filaments, and microtubules. The microtubule network gives the cell its general shape by extending throughout the cell. Microtubules can support the cell, especially in long protrusions such as axons, because they are the most rigid of all the filaments with a persistence length of about 1 mm (Hawkins *et al* 2010, 2012, 2013). Structurally, microtubules are hollow protein tubes made from a lattice of alpha/beta tubulin heterodimers. The cross-sectional diameter of microtubules is 25 nm, and they can be 1–100 μm in length. After nucleation of a short tube, the microtubule filament can grow by adding subunits to the ends. Because the basic building block is a heterodimer the entire microtubule structure is physically polarized such that the two ends are distinct (figure 1(a)). The end exposing the beta tubulin grows faster and is called the plus-end; the alpha-exposed end is called the minus-end.

In cells, microtubule networks are often bundled. Because the microtubules have a polarity, the bundles can be composed of parallel arrays, where all the microtubules have the same polarity, antiparallel arrays, where the polarity of the microtubules alternate, or random arrays of microtubules (figure 1(b)). In cells, parallel and antiparallel arrays are specifically organized and arranged to perform different functions. These specific bundles are created by motors and microtubule-associated proteins (MAPs). For instance, parallel bundles are required in the kinetochore fibers of the mitotic spindle to perform work, whereas overlapping microtubules at the edges of the spindle enable pushing forces.

The MAP65/PRC1/Ase1 family of proteins is known to be important for the formation of antiparallel microtubule bundles in metaphase, telophase, and cytokinesis (Jiang *et al* 1998, Schuyler *et al* 2003, Yamashita *et al* 2005, Loïodice *et al* 2005, Zhu *et al* 2006) and can form large bundles when ectopically expressed in interphase (Mollinari *et al* 2002). Prior work on this family of proteins has shown that MAP65 proteins crosslink microtubules with a 25 nm distance by dimerizing across the interstitial space between microtubules (Chan *et al* 1999, Gaillard *et al* 2008). These crossbridges between the two microtubules are regularly spaced at high concentration with 35 nm periodicity (Chan *et al* 1999, Gaillard *et al* 2008). At low concentrations or regions of microtubules that are not adjacent to another microtubule, MAP65 are irregularly spaced and the crossbridge portion of the protein is flexible (Subramanian *et al* 2010). Previous work has also shown that MAP65 binding, while bundling very efficiently, does not hinder microtubule dynamic instability or the motility of crosslinking motors, such as Eg5 (Tulin *et al* 2012, Subramanian *et al* 2010, Bieling *et al* 2010). This is because MAP65 has a short residence time on the microtubule both in cells (Jiang *et al*

1998, Loïodice *et al* 2005) and *in vitro* (Subramanian *et al* 2010, Bieling *et al* 2010, Tulin *et al* 2012, Kapitein *et al* 2008). The residence time is increased by bundling, yet is still relatively short for such a potent bundler (Subramanian *et al* 2010, Bieling *et al* 2010, Tulin *et al* 2012, Kapitein *et al* 2008). Interestingly, there is a specific range of angles between two microtubules over which MAP65 interacts and causes bundling. If the angle is too large or small, MAP65 is unable to bundle (Tulin *et al* 2012).

In order to explore the effect a specific antiparallel crosslinker will have on the organization of microtubules, we performed simple microtubule gliding assays propelled by kinesin-1 motor proteins. First, we determined the phase diagram for MAP65 induced microtubule bundling as a function of increasing numbers of microtubules and increasing MAP65 concentration. Next, we performed gliding assays with MAP65 added to the chamber after microtubules were gliding or by adding microtubules bundled by MAP65 before introduction to the chamber. Interestingly, the kinesin motors were stopped by adding high concentrations of MAP65 to gliding microtubules, despite the rapid dissociation of MAP65 from single microtubules. On the other hand, pre-bundling of microtubules led to novel self-organization of microtubules that were pulled apart and rebundled during the gliding assay. We used two-color imaging in total internal reflection fluorescence to visualize GFP-MAP65 proteins during microtubule gliding. As expected, antiparallel bundles showed a high concentration of GFP-MAP65 during gliding.

2. Experimental details

Full experimental details are in the supplemental material (available at stacks.iop.org/JPhysCM/25/374103/mmedia). We purified a kinesin-1 construct (KIF5B truncated at amino acid 560) fused to a C-terminal HaloTag (Promega) and 6× Histidine (6× His) tag according to (Pierce and Vale 1998, Conway *et al* 2012). Tubulin was made by standard procedures and purified to 97% using a high concentration of PIPES to remove most charged associated proteins (Peloquin *et al* 2005). Tubulin was fluorescently labeled using a DyLight-650 (Pierce) antibody labeling kit as described previously (Hyman *et al* 1991).

To polymerize and stabilize fluorescent microtubules for assays, we mixed 45 μM labeled tubulin with 45 μM unlabeled tubulin and centrifuged at 298 000×g for 10 min at 4 °C to remove tubulin aggregates. The supernatant was incubated at 37 °C for 20 min with 1 mM guanosine triphosphate (GTP) to polymerize tubulin. Microtubules were stabilized with 50 μM Taxol and incubated for 20 min at 37 °C. Formed microtubules were centrifuged at 14 000×g for 10 min at 25 °C, and the pellet was resuspended in 50 μl of PEM-100 (100 mM Na-PIPES, 1 mM $MgSO_4$, 1 mM EGTA, pH 6.8) with 50 μM Taxol.

Unlabeled MAP65 and GFP-MAP65 constructs were provided from the Dixit Lab and were purified using a 6× His tag, as previously described (Tulin *et al* 2012). We tested the ability of MAP65 to bundle microtubules by incubating 0.45 μM, 4.5 μM, or 22.5 μM tubulin with MAP65 at 1:0, 1:0.1, 1:1, 1:2, 1:3, and 1:8 molar ratios (tubulin:MAP65). Using the known K_D value for MAP65 and GFP-MAP65 of ~1.2 μM (Tulin *et al* 2012), we deduced the ratio of bound MAP65 to be 0%, 3%, 22%, 41%, 51%, and 76% for each of these molar ratios, respectively. Microtubules were incubated with MAP65 for 30 min at room temperature. Bundled microtubules were flowed into a flow chamber made from a slide, cover glass, and double stick tape to create a path 5 mm wide, as previously described (Liu *et al* 2011). The slide and cover glass were biologically cleaned, and the chamber holds ~10 μl. Microtubules were visualized using epi-fluorescence with the same exposure and gain settings to allow comparison between images. To visualize MAP65 binding, GFP-MAP65 was used and imaged in epi-fluorescence in the green channel. Co-localization of GFP-MAP65 with microtubule bundles is indicative of functional MAP65.

Single molecule binding of MAP65 was performed by adhering single microtubules to a silanized cover glass in a flow chamber using anti-tubulin antibodies, as previously described (Dixit and Ross 2010, Díaz-Valencia *et al* 2011, Conway *et al* 2012). Microtubule gliding assays were performed in two ways: (1) microtubules were flowed in and began gliding before MAP65 was added, similar to our previous report (Liu *et al* 2011), or (2) microtubules and MAP65 were premixed before being added into the chamber. For both, kinesin was added first and incubated for 5 min. The chamber was next washed with wash buffer (5 mg ml^{-1} BSA, 60 μM Taxol, 20 mM DTT in PEM-100) to remove excess kinesin that did not adhere to the cover glass and block the cover glass with BSA (figure 1(d)). Kinesin walks toward the plus-end of the microtubule causing the microtubule to be propelled with its minus-end in front.

For gliding assay type (2), fluorescent microtubules (225 nM) were flowed into the chamber and activation mix was added to check for motility. Separately, fluorescent microtubules (4.5 μM) were incubated for 10 min with 22% MAP65 where 2% of the MAP65 was GFP-MAP65. After incubation, activation mix was added to the microtubules and MAP65, diluting the microtubules to 450 nM final concentration. The diluted microtubule-MAP65 solution was added to the chamber and imaged in epi-fluorescence as described above.

Epi-fluorescence and single molecule imaging were performed on a Nikon Ti–U using an Orca CCD (Hamamatsu) or a Cascade electron multiplier CCD (EM-CCD, Roper), or an IXON EM-CCD (Andor). All images were exported from Nikon Elements as .tif files and imported into ImageJ for analysis. Movies were recorded as .nd2 files and opened in ImageJ with the LOCI plug-in (http://loci.wisc.edu/bio-formats/imagej). All pixel to micron ratios are determined with a micrometer to show that the 60× water coupled objective yields 0.108 μm/pixel for the Orca camera and 270 nm/pixel for the EM-CCD cameras.

Images of microtubule bundles were analyzed in ImageJ. The intensity of the microtubules, bundles, and GFP-MAP65 were measured by drawing a region of interest perpendicular to the bundle. The intensity profile was recorded and plotted in KaleidaGraph and fit with a Gaussian function:

$y = A\exp(-\frac{1}{2}(\frac{x-x_0}{\sigma})^2)$, where A is the amplitude, x_0 is the center of the peak, and σ is the standard deviation. The amplitudes were recorded to report on the number of microtubules in the bundle. Images with 0% and 3% MAP65 had single microtubules present that were used to determine the intensity of single filaments. The amplitudes of the bundles were divided by the average intensity of single filaments to determine the number of microtubules in the bundle.

For microtubule gliding assays, velocities and angles were measured in ImageJ. Velocities were measured using the plug-in MTrackJ (www.imagescience.org/meijering/software/mtrackj/). Angles were recorded using the angle measure tool in ImageJ. Angles between two intersecting microtubules were measured when the microtubules first encountered each other and two frames later, as described in figure 1(e). The angle of entry between two microtubules just as they encounter each other was measured by drawing a line tangent to one microtubule from the plus-end (trailing end) to the intersection and then to the tangent to the plus-end (trailing end) of the second microtubule. The angle of exit between two microtubules just after they encounter each other was measured by drawing a line tangent to one microtubule from the minus-end (leading end) to the intersection and then to the tangent to the minus-end (leading end) of the second microtubule.

3. Results and discussion

3.1. Bundling by MAP65

We examined the bundling activity of MAP65 as a function of concentration with increasing concentrations of microtubules. At low concentrations of microtubules (450 nM) and MAP65 (0, 3%), the microtubules do not bundle, but stay as single microtubules (figure 2(a)). This is reasonable, since so few microtubules would not be likely to come into contact due to thermal fluctuations. Even moderate and high concentrations of microtubules (4.5 μM and 22 μM) are not bundled without MAP65 (0%). Thus, the bundling is not due to depletion forces or liquid crystalline alignment at these concentrations.

At intermediate MAP65 concentrations (22%, 41%), the microtubules at the lowest concentration (450 nM) make 'straight bundles' where many microtubules are bundled together in shorter, straighter bundles (figure 2). This is similar to previously visualized bundles (Chan *et al* 1999, Wicker-Planquart *et al* 2004, Smertenko *et al* 2004, Gaillard *et al* 2008), which use low microtubule concentrations. We measured the intensity across the microtubule, and fit the profile to a Gaussian. We normalized the amplitude of the measured intensity of bundles to the intensity of single microtubules, as seen in the 0% data (figure 3(a)) to obtain the number of microtubules per bundle. We report average values from multiple measurements across bundles. It is clear that there are multiple microtubules within the bundle and the number of microtubules per bundle increases linearly with increasing MAP65 concentration (figure 3(b)).

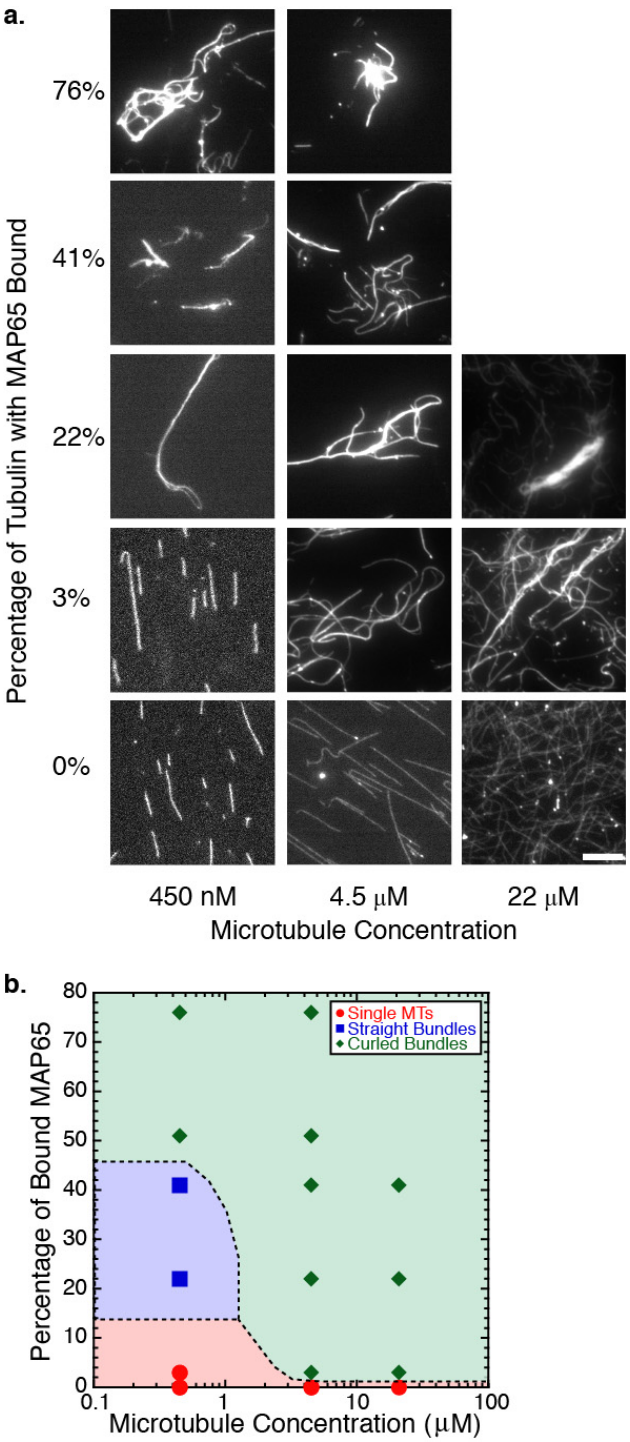

Figure 2. Phase diagram of MAP65 induced bundles. (a) Representative images of microtubule bundles with increasing amounts of MAP65 and microtubules. Scale bar is 10 μm for all images. (b) Phase diagram of the types of bundles formed as a function of MAP65 concentration and microtubule concentration. Microtubules appear to be single microtubules (red circles), short, straight bundles (blue squares), or large, curled bundles (green diamonds). The background color represents the possible region for each phase.

At high concentrations of MAP65 (76%) but low microtubule concentrations, we see microtubule bundles that are large enough to bend around and curl back on themselves

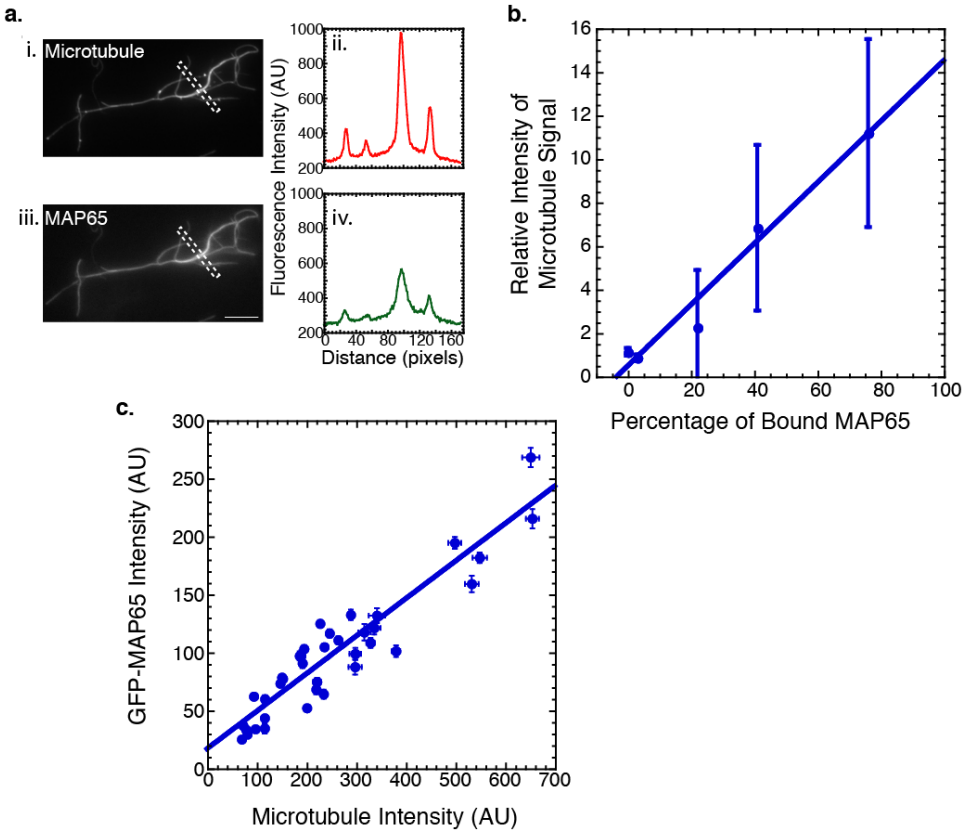

Figure 3. MAP65 binding and number of microtubules in bundles. (a) Example image of microtubule bundle with 4.5 μM microtubules and 22% GFP-MAP65. (i) Rhodamine-labeled microtubules and (iii) GFP-MAP65 bound to the microtubules are clearly visible. Scale bar is 10 μm for both images. Intensity scans perpendicular to the bundle in the region outlined show that the intensity of (ii) microtubules and (iv) GFP-MAP65 are proportional implying that MAP65 is coating the microtubule. (b) The intensity of microtubules in bundles increases linearly with increasing MAP65 concentration for microtubule concentration of 450 nM. Using the intensity of the single microtubules at 0% and 3% MAP65, we estimated the number of microtubules in the bundles (y-axis) at higher concentrations of MAP65. Large error bars are the result of bundles with different numbers of microtubules, as seen in (a). The best linear fit has a slope of 0.14 ± 0.01 and intercept of 0.5 ± 0.6 with a goodness of fit equal to $R^2 = 0.97$. (c) Relative intensity of the microtubule (x-axis) and GFP-MAP65 (y-axis). The amount of GFP-MAP65 binding is linearly proportional to the number of microtubules in the bundle, and can be fit with a linear equation with slope 0.32 ± 0.02. The goodness of fit is $R^2 = 0.87$.

(figure 2(a)). We call these bundles 'curled bundles.' High microtubule concentrations (4.5 μM and 45 μM) have curled bundles even at low MAP65 concentrations (3%), and there are proportionally more microtubules in the cross-section of each bundle (figure 3).

Using this data, we can create a phase diagram of the types of bundles induced by MAP65 as a function of microtubules and MAP65 concentration (figure 2(b)). We found that the order of addition of MAP65 did not matter to the formation of the bundles of different types. Thus, if MAP65 was present during polymerization of the tubulin dimers into filaments, we had the exact same phase diagram as when the microtubules were polymerized prior to incubation with MAP65. We examined the location of MAP65 on the bundles in epi-fluorescence using GFP-MAP65, and found that the bundles were coated with MAP65 in all instances, and the binding was obvious above background levels, as expected (figure 3(a)). Further, for low concentrations (3%, 22%, 41%) the amount of GFP-MAP65 was linear with the number of microtubules in the bundle (figure 3(c)). We expect the concentration of bound MAP65 to be linearly proportional to the number of microtubules in the bundle for binding ratios below 50%, because this is the linear regime for binding.

3.2. Single microtubule gliding

Next, we tested the ability of MAP65 to alter the organization of microtubules when added to a microtubule gliding assay powered by kinesin motors. We performed the experiment in two ways: (1) allowing the microtubules to glide as individual filaments and then adding MAP65 to the chamber, or (2) pre-bundling the microtubules with MAP65 and then adding the bundles to the kinesin chamber.

When MAP65 was added to a chamber with microtubules (450 nM) that were already gliding, the velocity decreased with increasing concentrations of MAP65 (figure 4(a)). At low MAP65 concentration (3%) gliding velocity did not decrease. At intermediate MAP65 concentrations (22% and 41%) gliding was slowed, but clear. At high MAP65 concentrations (51% and 76%) no microtubules were able to glide. We examined each chamber prior to adding the MAP65, and all were able to glide before MAP65 was added. In order to

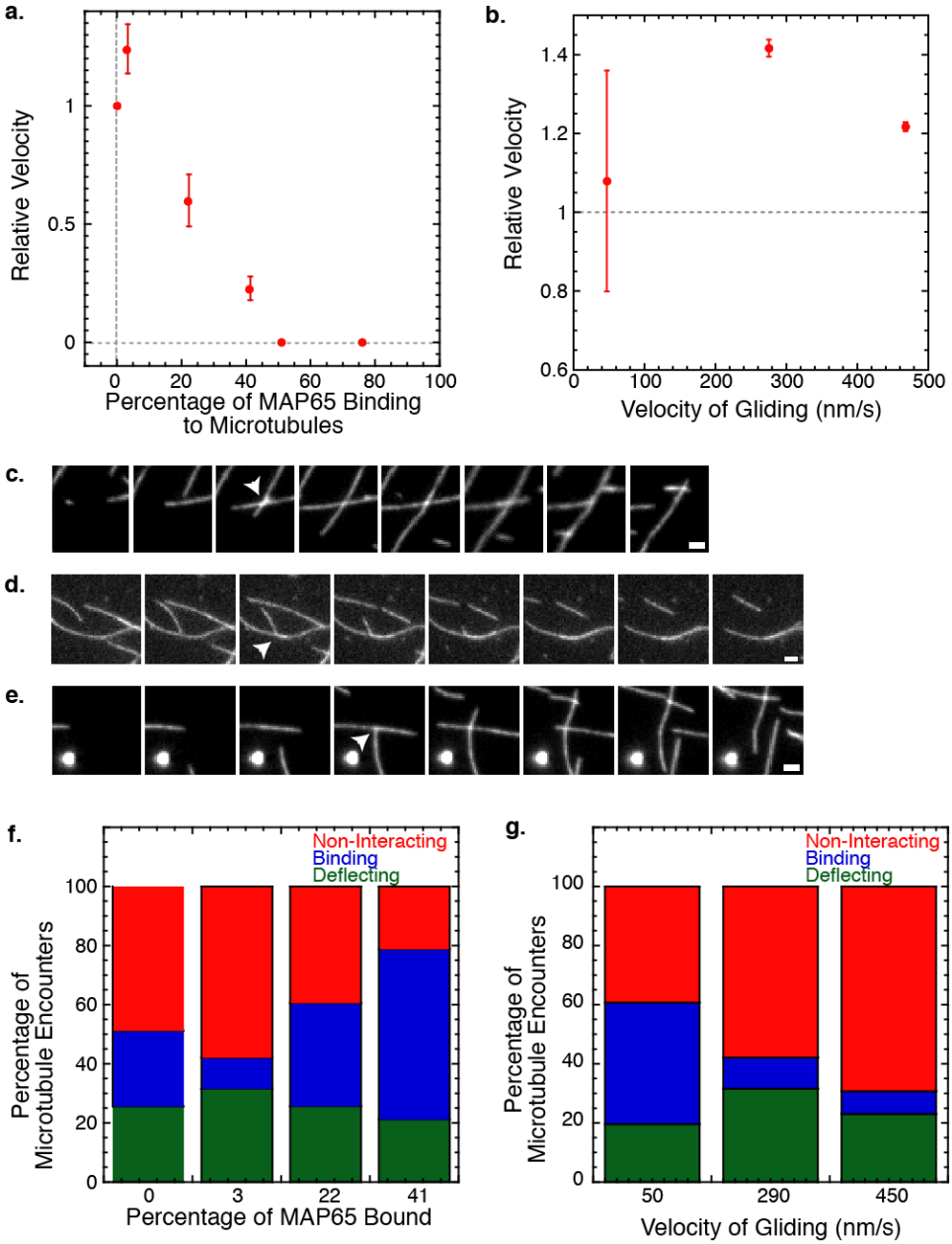

Figure 4. Velocity and interaction between microtubules as a function of MAP65 concentration and gliding velocity. (a) The velocity of gliding microtubules relative to same chamber controls as a function of added MAP65. (b) The velocity of gliding microtubules relative to same chamber controls as a function of control velocity for 3% MAP65 added to the chamber. For all gliding velocities, the average velocity with 3% MAP65 added is faster than the velocity of gliding in the same chamber before MAP65 was added. (c) Time series of example encounter (arrowhead) between two single microtubules that are 'non-interacting.' The time between frames is 2 s. The incoming angle is the same as the outgoing angle between the microtubules to within 10°. (d) Time series of example encounter (arrowhead) between two single microtubules that are 'binding.' The time between frames is 2 s. The microtubules go off together such that exiting angle is 0°. (e) Time series of example encounter (arrowhead) between two single microtubules that are 'deflecting.' The time between frames is 4 s. The exit angle changes by 15° compared to the entry angle for this example. Scale bar is 2 μm for all images. (f) Percentage of microtubule encounters that are non-interacting (red bars), binding (blue bars), or deflecting (green bars) for increasing concentrations of MAP65. (g) Percentage of microtubule encounters that are non-interacting (red bars), binding (blue bars), or deflecting (green bars) for increasing gliding velocities for 3% MAP65.

avoid confusion and compounding effects, we only tracked single microtubules that were clearly separate from other neighboring filaments. The reported velocities are the average velocity of gliding over the entire time the microtubule is discernable as a single microtubule. Any interactions that slow the velocity are averaged into the reported velocities.

Interestingly, the behavior of microtubule gliding follows the phase behavior of microtubule bundling. For 450 nM microtubules, both 0% and 3% MAP65 had no bundling effect (figure 2). Thus, there was not enough MAP65 to bundle microtubules together and overpower the thermal fluctuations. In this regime, we would not expect the

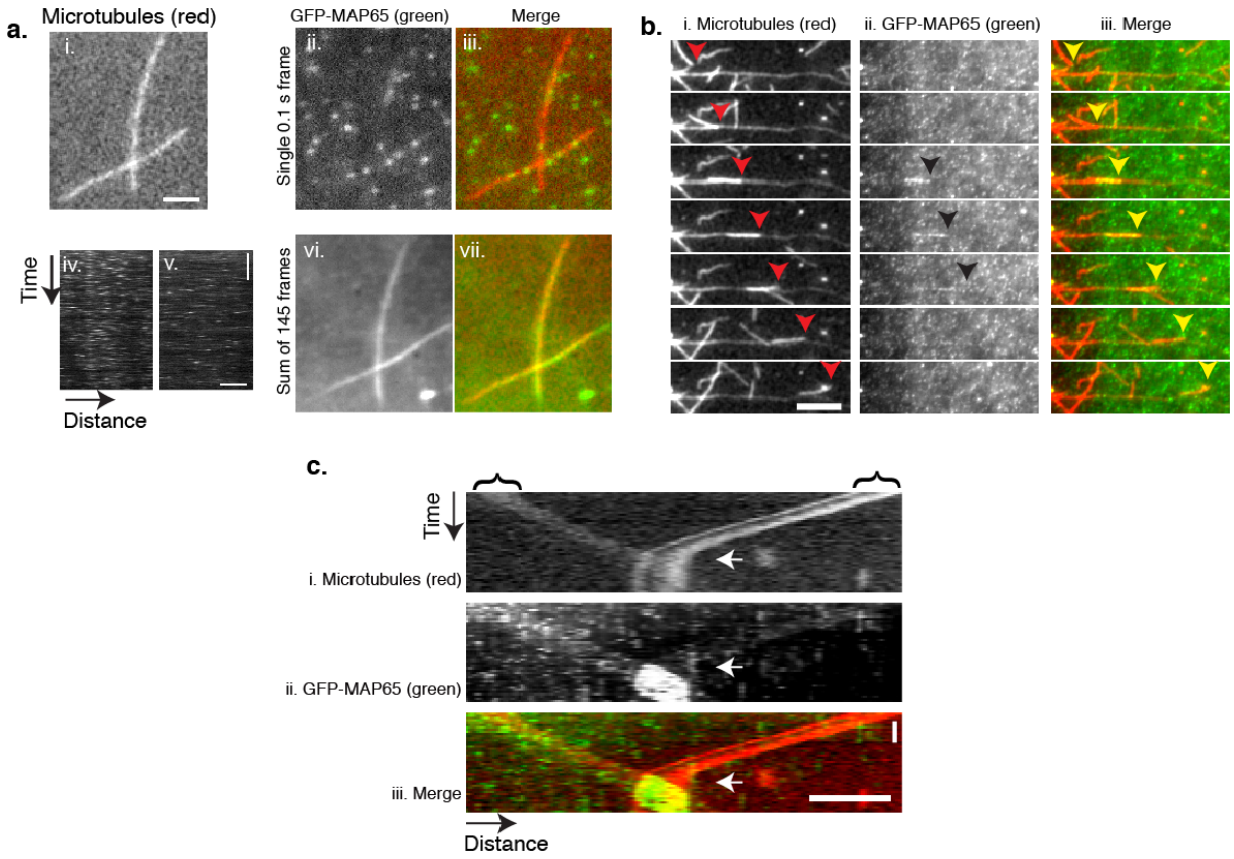

Figure 5. GFP-MAP65 binding to single microtubules and during gliding. (a) Single molecule GFP-MAP65 binding to individual microtubules. (i) Dylight-650 microtubules imaged in epi-fluorescence. Scale bar 2 μm for frames (i), (ii), (iii), (vi), and (vii). (ii) GFP-MAP65 molecules imaged in TIRF microscopy. (iii) Merge of microtubule image (i, red) and GFP-MAP65 image (ii, green) shows single MAP65 molecules binding to the microtubules and to the cover glass. (iv) Kymograph of GFP-MAP65 binding to a microtubule with positive time moving vertical downward and positive distance in the horizontal direction. Individual GFP-MAP65 molecules appear to bind for only a single 100 ms frame. (v) Kymograph of GFP-MAP65 binding to the cover glass. The vertical scale bar is 2 s and the horizontal scale bar is 2 μm for both kymographs in (iv) and (v). (vi) Sum of 145 100 ms frames of single molecule GFP-MAP65 imaged with TIRF as seen in (ii). (vii) Merge of microtubule image (i, red) and GFP-MAP65 summed image (vi, green) shows that the GFP-MAP65 binds to the microtubule preferentially over the cover glass. (b) When two antiparallel microtubules encounter and bind during gliding, GFP-MAP65 accumulates between them. (i) Time series of Dylight-650 microtubules gliding. The red arrow indicates the front end of the shorter microtubule that moves from left to right. Time between frames is 4 s. Scale bar is 10 μm for all images. (ii) Same time series as shown in (i) depicting the GFP-MAP65 using TIRF. Black arrows highlight the front of the enrichment of GFP-MAP65 when the two microtubules are within 35 nm. (iii) Merged image of microtubules in red and GFP-MAP65 in green. Yellow arrows indicate the front end of the shorter microtubule moving from left to right. A movie of this encounter can be found in the supplemental movies (available at stacks.iop.org/JPhysCM/25/374103/mmedia). (c) Kymographs of two microtubules encountering each other showing accumulation of GFP-MAP65 and reduction of speed when they overlap. (i) Kymograph of two microtubules approaching from opposite sides. Curly brackets at the top denote the starting position of the two microtubules. The positive time direction is downward. As time progresses, the two microtubules move toward each other in space (the horizontal axis). When they overlap, the velocity decreases (white arrow). Vertical lines in the kymograph denote no movement. (ii) Kymograph of the same encounter as shown in (i) depicting the GFP-MAP65 using TIRF. When the two microtubules overlap, there is a large signal increase in the GFP-MAP65 signal (white arrow). (iii) Merged image of microtubules in red and GFP-MAP65 in green. It is clear that the enhanced MAP65 binding occurs when the microtubules overlap and slow down (white arrow). Vertical scale bar is 20 s in time. Horizontal scale bar is 10 μm in space. A movie of this encounter can be found in the supplemental movies (available at stacks.iop.org/JPhysCM/25/374103/mmedia).

MAP65 to have much effect on kinesin gliding (figure 4(a)). Interestingly, for 3%, we see a robust result that addition of MAP65 increased the velocity 7–40% above the control velocity measured in the same chamber using the same microtubules and kinesin (figure 4(c)). Presumably, a small amount of MAP65 binding is reducing the drag on the gliding microtubule, but we do not know the mechanism. This is an interesting avenue for future studies with MAP65.

At intermediate MAP65 concentrations (22% and 41%), the phase diagram showed straight bundles (figure 2). This data implies that there is enough MAP65 to maintain bundles together despite thermal fluctuations. From intensity measurements, we estimate that there are 2 to 10 microtubules in cross-sections of these bundles (figure 3(b)). In our gliding assay, we started with unbundled, gliding filaments, and we only track single microtubules. Nevertheless, as microtubules encounter each other during gliding, they are more likely

to interact with these higher levels of MAP65, and this interaction results in a reduced velocity (figure 4(a)). This is clearly observed in the kymographs shown in figure 5(c), where two microtubules glide toward each other and slow down when they overlap. It should be noted that there were very few single microtubules gliding at 41% MAP65. Most were in bundles and not distinguishable as single microtubules.

At the highest concentrations of MAP65 (51% and 76%), we observed no motion of single microtubules. These are the same concentrations that displayed curled bundles with 450 nM microtubules. These microtubules are likely to be highly crosslinked and therefore the most hindered by MAP65 binding. Previous work also saw a slow down of microtubule motors in the presence of Ase1/PRC1 in cells and *in vitro* (Janson *et al* 2007, Subramanian *et al* 2010).

3.3. Two microtubule interactions

We quantified the types of interactions between microtubules that encounter each other during gliding as a function of increasing MAP65 concentration (0%, 3%, 22%, and 41%). We classified interactions based on the change in angle between two interacting microtubules before and after they encounter. We measured the angle the two microtubules made when they encountered each other with deference to the direction of the motion. Since microtubules gliding on kinesin motors glide with the minus-ends in front, we measured the angle from plus-end to intersection to plus-end of the second microtubule. If the angle is less than 90°, then the two microtubules are coming toward each other in a parallel orientation. If the angle is greater than 90°, then the microtubules are approaching as antiparallel. We also measured the angle exiting the intersection by measuring the angle from the minus-end to the intersection and to the minus-end of the second microtubule.

Microtubules that passed without any change in angle before or after the encounter ($\theta_{\text{entry}} - \theta_{\text{exit}} < 10°$) were classified as non-interacting (figures 1(e) and 4(c), supplemental movie 1 available at stacks.iop.org/JPhysCM/25/374103/mmedia). Microtubules that appear to overlap within the resolution of the microscope ($\theta_{\text{exit}} < 10°$ for parallel microtubules or $\theta_{\text{exit}} > 170°$ for antiparallel microtubules) after encountering each other were classified as binding (figure 4(d), supplemental movies 2–3 available at stacks.iop.org/JPhysCM/25/374103/mmedia). Microtubules that had a change in angle after the encounter ($\theta_{\text{entry}} - \theta_{\text{exit}} > 10°$), but are not gliding together were classified as deflecting (figure 4(e), supplemental movie 4 available at stacks.iop.org/JPhysCM/25/374103/mmedia).

We found that the type of interactions changed with the increasing concentration of MAP65 (figure 4(f)). As expected, the percentage of encounters that were non-interacting decreased with increasing MAP65 concentration. In the absence of MAP65, about half the interactions were non-interacting, where two microtubules glided through each other. This result is interesting in light of our previous results with kinesin-powered transport under crowded conditions (Liu *et al* 2011), recently reviewed in Hancock (2012). We found that microtubules gliding at high concentrations were not able to align with liquid crystalline order, but rather had short-range order that caused looping (Liu *et al* 2011). This is in contrast to several prior results where actin–myosin gliding in crowded conditions showed that actin filaments align into liquid crystalline orders that are propelled by the myosin (Schaller *et al* 2010, Butt *et al* 2010). Large-scale defects in the alignment occur to create points about which the entire aligned pattern swirl. For microtubules, the alignment appears to depend on the motor. Axonemal dynein causes large-scale alignment of microtubules into large, looping bundles, but cytoplasmic dynein and kinesin-1 do not stimulate alignment (Sumino *et al* 2012, Liu *et al* 2011). Thus, for kinesin-driven motion, increased steric interactions due to high concentrations of filaments are not enough to drive alignment, as it is for axonemal dynein or actin–myosin.

The addition of MAP65 enhanced interaction between two microtubules. At 41% MAP65, the percentage of non-interacting pairs decreased to 20% (figure 4(f)). As fewer encounters were non-interacting, the percentage of microtubule pairs that were binding increased. In the absence of MAP65, about 25% of the encounters resulted in binding between the microtubules. At 41% MAP65, the majority of encounters, 60%, resulted in binding. This is to be expected, since we know MAP65 crosslinks microtubules, and the more MAP65 present, the more likely crosslinking is to occur. Thus, we can enhance the interactions between microtubules during kinesin-driven gliding using MAP65, and this could result in new microtubule patterns at higher microtubule concentrations.

We find that MAP65 can alter the velocity, so, we need to question if velocity also affects the interaction qualities. To quantify the effect of velocity on interaction ability, we measured the types of interactions for microtubule pair encounters as a function of velocity for 3% MAP65 (figure 4(g)). When the gliding velocity was slow (50 nm s^{-1}), the percentages of non-interacting (55%) and binding (20%) encounters are very similar to the case when there is no MAP65. At higher velocities (290 and 450 nm s^{-1}) the number of binding encounters is greatly reduced, and most encounters are non-interacting (60–70%). The dependence on the velocity implies that the MAP65 needs some time to crosslink the microtubules; the crosslinking activity is not instantaneous. This result implies that the binding time for MAP65 is likely short on single microtubules. Thus, there is a low probability that MAP65 is sitting on the gliding microtubules waiting for a second microtubule to encounter and cause crosslinking.

Interestingly, the percentage of microtubule pairs that deflected was fairly constant for all concentrations of MAP65 (24% $\pm$ 2% for all data sets). From this result, we conclude that deflection is an activity that is independent of MAP65. Deflection may be caused by random turning that is observed even with single microtubules gliding far from other microtubules.

Since MAP65 bundles microtubules in an antiparallel manner, two interacting microtubules are more likely to

interact and slow down if they are antiparallel during gliding. Previous studies have shown that the probability of bundling two polymerizing microtubules depends on the angle the two microtubules encounter one another, and that increasing amounts of MAP65 result in a larger distribution of angles that result in bundling (Tulin *et al* 2012). We sought to examine the angular dependence of the types of interactions. Our data showed that non-interacting microtubule pairs encountered each other at angles that are evenly distributed around perpendicular (supplemental figure 1(a) available at stacks.iop.org/JPhysCM/25/374103/mmedia). Binding interactions between microtubules occurred at acute or obtuse angles, but not perpendicular (supplemental figure 1(b) available at stacks.iop.org/JPhysCM/25/374103/mmedia). We did not see any significant differences in the entrance angles with or without MAP65. Thus, unlike in a polymerization assay, gliding microtubules do not have an angular dependence on interaction. This may be due to the larger forces on the microtubule by many kinesin motors during gliding that do not exist during polymerization.

3.4. Two microtubule crosslinking

The interactions we observed are likely enhanced by crosslinking of two antiparallel microtubules by MAP65. In order to observe the activity of MAP65 on stationary or gliding and interacting microtubules, we used two-color imaging of microtubules and GFP-MAP65. In our hands, MAP65 was only observed to bind for a single 100 ms frame (figure 5(a)). In a single frame using single molecule total internal reflection fluorescence (TIRF) imaging, GFP-MAP65 molecules are observed binding to both the microtubule and the glass near the microtubule (figure 5(a)(ii) and (iii)). We can show that the MAP65 is preferentially binding to the microtubule by creating a kymograph (space–time image) to display the binding of MAP65 to the microtubule (figure 5(a)(iv)). We can also compare the binding on the glass by creating a similar kymograph in a region of the chamber that has no microtubules (figure 5(a)(v)). It is clear from the kymograph that MAP65 is very dynamic, only binding for <200 ms on both the microtubule and the cover glass, but there are far more MAP65 molecules binding to the microtubule. Although the interaction was short-lived, it was specific to the microtubules. After summing the intensities of 145 frames, the microtubules are clearly visible (figure 5(a)(vi)), implying that the affinity of MAP65 for microtubules was higher than for the background glass. The ability of MAP65 to bind preferentially to the microtubules, but only bind for a short time explains why faster velocities would lead to fewer interactions. Previous studies showed that MAP65 has a short association time to single microtubules (Tulin *et al* 2012).

We can also image GFP-MAP65 during microtubule gliding (figures 5(b) and (c), supplemental movies 5–8 available at stacks.iop.org/JPhysCM/25/374103/mmedia). MAP65 is known to hold microtubules about 25–35 nm apart within bundles (Tulin *et al* 2012, Chan *et al* 1999, Gaillard *et al* 2008). Assuming that MAP65 must be within this range to crosslink microtubules, this is a long-range interaction, but it is below the resolution of our microscope. In order to test if the microtubules are truly being crosslinked during gliding, we performed two-color imaging of microtubules and GFP-MAP65 during gliding. The background MAP65 binding to the cover glass is very high because our normal blocking method for single molecule imaging prevented gliding. Thus, we used casein to block the surface and photobleached most of the MAP65 bound to the glass before imaging. Only 100 nM of the total 450 nM of MAP65 was GFP-labeled (22% MAP65). We found many examples of binding interactions during gliding. When the two binding microtubules were antiparallel, we observed an increase in GFP-MAP65 binding to the overlap region (figures 5(b), (c), and supplemental movies 1–4 available at stacks.iop.org/JPhysCM/25/374103/mmedia). The fact that the GFP-MAP65 was observed more at the overlap region implies that MAP65 has an even higher affinity for antiparallel bundles than single microtubules, as previously observed (Tulin *et al* 2012). Further, we can conclude that the MAP65 is crosslinking the two microtubules during gliding. Figure 5(b) shows a good example where the microtubules bind during gliding and GFP-MAP65 localizes to the microtubules when they are close enough. In frame 6 of the time series, the two microtubules are still antiparallel and appear to be very close, but we cannot detect the GFP-MAP65, implying that they are farther away than 35 nm.

In figure 5(c), we have created kymographs of the gliding microtubules and GFP-MAP65. In this case, the amount of GFP-MAP65 is very high when the two microtubules bind, suggesting that a high amount of MAP65 is between them. In this example, we see a significant reduction in the velocity after binding occurs, most likely due to this very high concentration of MAP65. The change in velocity implies that there is an added drag force due to the MAP65 crosslinking.

Before they encounter, the velocity is constant, so the forces are balanced, and we can find the drag coefficient from the motion:

$$-F_{\text{drag}} = F_{\text{motors}} \tag{1}$$

where F_{drag} is the drag force and F_{motors} is the force due to the motors. From the definition of drag force, we get:

$$bv_1 = N_{\text{motors}} F_{1\text{motors}} \tag{2}$$

where b is the drag coefficient with units of kg s^{-1}, v_1 is the velocity of the microtubule, N_{motors} is the number of motors acting on the filament, and $F_{1\text{motor}}$ is the stall force due to a single kinesin-1 motor. We know that one motor has a stall force of 5 pN from optical trapping measurements, and this gives us an upper bound estimate for the force (Svoboda *et al* 1993, Ross *et al* 2008). We can estimate the number of motors acting on a microtubule from an estimate of 500 motors μm^{-2}, surface density of motors and a projected surface area of a 10 μm microtubule to be 0.25 μm^2, as previously performed (Liu *et al* 2011). This gives about 125 motors on the microtubule. We can measure the average velocity from the kymograph by measuring the number of pixels it travels in the horizontal (distance) direction and the

conversion of 270 nm/pixel and dividing this number by the number of pixels in the vertical (time) direction and knowing that one pixel is 2 s. We find that the velocity before the two motors meet for the microtubule coming from right to left is 467 nm s^{-1}. From these estimates, we can estimate an upper bound for the drag coefficient acting on the microtubule before interacting:

$$\begin{aligned} b &= N_{\text{motors}} F_{1\text{motors}}/v_1 \\ &= (125 \text{ motors})(5 \text{ pN})/(467 \text{ nm s}^{-1}) \\ &= 1.3 \times 10^{-3} \text{ kg s}^{-1}. \end{aligned} \tag{3}$$

After the encounter, we approximate the velocity as constant, so the forces are balanced again, and we can find the drag coefficient for the motion due to MAP65. As above:

$$bv_2 = N_{\text{motors}} F_{1\text{motor}} \tag{4}$$

where v_2 is the new velocity after the encounter. We can estimate this new velocity and solve for the new drag coefficient:

$$\begin{aligned} b &= N_{\text{motors}} F_{1\text{motors}}/v_2 \\ &= (125 \text{ motors})(5 \text{ pN})/(135 \text{ nm s}^{-1}) \\ &= 4.6 \times 10^{-3} \text{ kg s}^{-1}. \end{aligned} \tag{5}$$

We can compare the drag coefficients we estimated for microtubule transport without and with MAP65 to the drag force on a 1 μm bead moving in water:

$$\begin{aligned} b_{\text{water}} &= 6\pi\eta r = 6\pi(10^{-3} \text{ kg ms}^{-1})(0.5\ \mu\text{m}) \\ &= 9.4 \times 10^{-9} \text{ kg s}^{-1}. \end{aligned} \tag{6}$$

As might be expected, the drag on a microtubule during gliding is much higher (6 orders of magnitude) than the drag on a 1 μm bead diffusing. The addition of MAP65 increases the drag 3.5-fold. Although this seems small, we have over-estimated the drag before overlapping. The motors are not likely exerting the maximum stall force before overlap, but are more likely to be close to stalling during the overlap. These considerations imply that 3.5 is a lower bound for the increase in drag with and without MAP65 binding. It may not be surprising considering that the increase in drag is relatively small given that the MAP65 is rapidly associating and dissociating, as shown in figure 5(a). Previous cellular studies showed this slow down was proportional to the overlapping length of the two microtubules (Janson *et al* 2007). Although we performed a simplified analysis with a constant velocity in the overlapping regions, we did see the velocity decrease as the amount of overlapping microtubules increased (figure 5(c)), in agreement with previous work.

3.5. Many microtubule organizations

In the previous experiments, we examined the effect of MAP65 on single microtubule gliding and two microtubule interactions. In this section, we begin to explore if kinesin motors could pull apart microtubules bundled by MAP65 before being added to the chamber. We used 22% MAP65 and 4.5 μM microtubules to create curled bundles (figure 2).

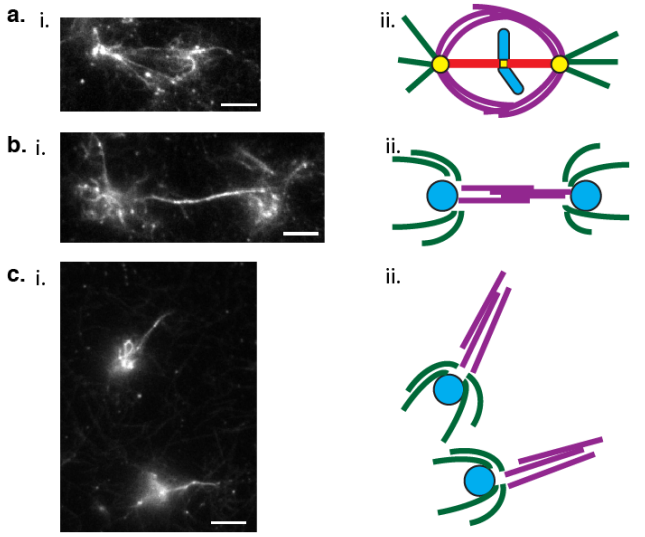

Figure 6. Cell-like structures made by adding MAP65 to microtubules before gliding. (a) Mitotic spindle networks. (i) Organization of microtubules and MAP65 being moved by kinesin motors on the surface that appears similar to the overlapping microtubule network around a mitotic spindle. (ii) Cartoon of the microtubule arrays found in mitosis. Red lines represent parallel microtubule bundles of the kinetochore fibers. Green lines represent astral arrays of microtubules pointing to the cell periphery. Purple lines represent the overlapping microtubule array around the spindle. Yellow dots represent the microtubule organizing centers/spindle poles. Blue bars represent the chromosomes. (b) Cytokinetic networks. (i) Organization of microtubules and MAP65 that appears similar to the cytokinesis microtubule network between two newly divided cells. (ii) Cartoon of microtubules in cytokinesis. Green lines represent astral array of new interphase network of microtubules. Purple lines represent interdigitating array of microtubules between two daughter cells. Blue circles represent nuclei of new daughter cells. (c) Migrating cell networks. (i) Organizations of microtubules and MAP65 that appear similar to migrating neuronal cells. (ii) Cartoon of microtubule arrays in migrating neuronal cells. Green lines represent astral arrays of microtubules in the cell body. Purple lines represent parallel arrays of microtubules in the axonal process that lead the way of migration. Movies of these networks dynamically rearranging can be found in the supplemental movies (available at stacks.iop.org/JPhysCM/25/374103/mmedia). Scale bars are equal to 10 μm for all images.

These microtubules were added to a chamber of kinesin that was able to glide microtubules, tested using 225 nM microtubules without MAP65. We found that kinesin was capable of pulling apart bundled microtubules.

Interestingly, the shape of the bundles had phenomenologically similar patterns to microtubule cytoskeletal networks observed in cells. We found organizations that appeared similar to the overlapping microtubule network of the mitotic spindle and motile cells (figure 6, supplemental movies 9–12 available at stacks.iop.org/JPhysCM/25/374103/mmedia). Microtubules of the mitotic spindle are organized into three distinct, yet interacting and essential networks (depicted in figure 6(a)(i)). The most prominent microtubules inside the spindle are the kinetochore fibers. They connect the spindle pole, where the microtubule minus-ends are gathered, to the chromosomes at the kinetochore. These parallel bundles of microtubules harness the work of microtubule

polymerization and depolymerization to cause movement of the chromosomes first to align them in metaphase and then to pull the sister chromatids apart in anaphase. The second network is the astral array that connects the spindle pole to the cell periphery. The function of the astral array of microtubules is to keep the spindle in the middle of the cell during division (or off-center for asymmetric divisions of certain cell types) so that the daughter cells are two equal-sized compartments. The network most resembling the network formed in our *in vitro* reconstitution assay is the overlapping array of microtubules that extends between the spindle poles and overlaps around the spindle (Zhu *et al* 2006) (figure 6(a), supplemental movie 9 available at stacks.iop.org/JPhysCM/25/374103/mmedia). In cells, these overlapping microtubules are crosslinked by MAP65 analogs (Ase1 or PRC1) and slid apart by tetrameric Eg5 motors. It is interesting that one of the organizations we found in our assay resembles the microtubule network where MAP65 functions in cells.

Another place during the cell cycle where MAP65/PRC1 plays a role is in the interdigitating network of microtubules that reach between two dividing cells during telophase and create the final microtubule bundle between two cells in the last stages of cytokinesis (Zhu *et al* 2006). Again, we find that one of the arrangements we observe in our system is similar to a cytokinesis-like arrangement (figure 6(b), supplemental movie 10 available at stacks.iop.org/JPhysCM/25/374103/mmedia). In cytokinesis, a bundle of antiparallel microtubules with PRC1 bound stretches between two daughter cells that are almost in interphase. Our system displays a similar bundle stretching between two networks of microtubules. As the kinesin pushes the microtubules, the bundle stretches and the two 'cell-like' networks get farther apart (supplemental movie 10 available at stacks.iop.org/JPhysCM/25/374103/mmedia). Previous work in fission yeast has shown that a minimal system composed of microtubules, Ase1 (MAP65, antiparallel bundler), Mto1 (nucleator), and klp2 (kinesin motor) is enough to establish a cell-like microtubule network of overlapping microtubules in cells without a nucleus (Carazo-Salas and Nurse 2006, Daga *et al* 2006). This mini-cell system was not as minimalistic as the reconstituted system we created here.

In addition to cell-cycle networks, we also observe networks that are similar to migrating cells or cilia (figure 6(c), supplemental movie 12 available at stacks.iop.org/JPhysCM/25/374103/mmedia). Although PRC1 is known to be a mitotic protein, a recent paper has shown that several central spindle/midbody proteins, including PRC1 localize in specific patterns at the basal body complex and are functional in ciliated epithelial cells. Thus, the cilia-like structures are also likely physiologically relevant. Further, other recent reconstitution experiments have recreated cilia-like microtubule bundles using kinesin-1 motors and depletion forces (Sanchez *et al* 2011). They found that these artificial cilia form and beat at air–liquid interfaces and are hydrodynamically coupled.

Although the experiments with pre-bundled microtubules are phenomenological, the resulting active networks are similar to those observed in cells during mitosis and cell motility. With our simple, minimalistic model system of microtubules, antiparallel crosslinkers, and stationary kinesin motors, we can recreate cell-mimetic networks. The kinesin motors add energy to the system to enable the reorganization of the microtubules in the networks. Various crosslinkers can be used in the future to examine different cellular networks in this minimal, yet powerful experimental system. Further, unlike prior exciting systems, our minimal system has a number of organizations formed. With our system, there is a possibility that the condensed organizations could change between these different organizations, similar to how cells perform morphology and organizational changes during the cell cycle. This future work will enable us to address questions of how cells organize their interior using the self-assembling organization principles of non-equilibrium, condensed matter physics.

Acknowledgments

We thank Ram Dixit for the MAP65 and GFP-MAP65 constructs and for the protocol to purify these proteins. We would like to thank Megan Bailey and Daniel Diaz for help with the tubulin labeling. We would like to thank Mike Gramlich for thoughtful discussions. JP was supported in the summer by National Science Foundation (NSF) Research Experience for Undergraduates grant CMMI-1242786. This work was also supported in part by NSF grants DBI-0923318 and CMMI-0928540 to JLR, MRSEC DMR-0820506 to the University of Massachusetts, and a Cottrell Scholars Award from Research Corporation for Science Advancement to JLR.

References

Bieling P, Telley I A and Surrey T 2010 A minimal midzone protein module controls formation and length of antiparallel microtubule overlaps *Cell* **142** 420–32

Butt T, Mufti T, Humayun A, Rosenthal P B, Khan S, Khan S and Molloy J E 2010 Myosin motors drive long range alignment of actin filaments *J. Biol. Chem.* **285** 4964–74

Carazo-Salas R E and Nurse P 2006 Self-organization of interphase microtubule arrays in fission yeast *Nature Cell Biol.* **8** 1102–7

Chan J, Jensen C G, Jensen L C, Bush M and Lloyd C W 1999 The 65-kDa carrot microtubule-associated protein forms regularly arranged filamentous cross-bridges between microtubules *Proc. Natl Acad. Sci. USA* **96** 14931–6

Conway L, Wood D, Tüzel E and Ross J L 2012 Motor transport of self-assembled cargos in crowded environments *Proc. Natl Acad. Sci. USA* **109** 20814–9

Daga R R, Yonetani A and Chang F 2006 Asymmetric microtubule pushing forces in nuclear centering *Curr. Biol.: CB* **16** 1544–50

Díaz-Valencia J D, Morelli M M, Bailey M, Zhang D, Sharp D J and Ross J L 2011 Drosophila katanin-60 depolymerizes and severs at microtubule defects *Biophys. J.* **100** 2440–9

Dixit R and Ross J L 2010 Studying plus-end tracking at single molecule resolution using TIRF microscopy *Methods Cell Biol.* **95** 543–54

Gaillard J, Neumann E, Van Damme D, Stoppin-Mellet V, Ebel C, Barbier E, Geelen D and Vantard M 2008 Two microtubule-associated proteins of Arabidopsis MAP65s promote antiparallel microtubule bundling *Mol. Biol. Cell* **19** 4534–44

Hancock W O 2012 Cytoskeletal organization: whirling to the beat *Curr. Biol.: CB* **22** R493–5

Hawkins T L, Mirigian M, Li J, Yasar M S, Sackett D L, Sept D and Ross J L 2012 Perturbations in microtubule mechanics from tubulin preparation *Cell. Mol. Bioeng.* **5** 227–38
Hawkins T, Mirigian M, Selcuk Yasar M and Ross J L 2010 Mechanics of microtubules *J. Biomech.* **43** 23–30
Hawkins T L, Sept D, Mogessie B, Straube A and Ross J L 2013 Mechanical properties of doubly-stabilized microtubule filaments *Biophys. J.* **104** 1517–28
Hyman A, Drechsel D, Kellogg D, Salser S, Sawin K, Steffen P, Wordeman L and Mitchison T 1991 Preparation of modified tubulins *Methods Enzymol.* **196** 478–85
Janson M E, Loughlin R, Loïodice I, Fu C, Brunner D, Nédélec F J and Tran P T 2007 Crosslinkers and motors organize dynamic microtubules to form stable bipolar arrays in fission yeast *Cell* **128** 357–68
Jiang W, Jimenez G, Wells N J, Hope T J, Wahl G M, Hunter T and Fukunaga R 1998 PRC1: a human mitotic spindle-associated CDK substrate protein required for cytokinesis *Mol. Cell* **2** 877–85
Kapitein L C, Janson M E, van den Wildenberg S M, Hoogenraad C C, Schmidt C F and Peterman E J 2008 Microtubule-driven multimerization recruits ase1p onto overlapping microtubules *Curr. Biol.* **18** 1713–7
Liu L, Tüzel E and Ross J L 2011 Loop formation of microtubules during gliding at high density *J. Phys.: Condens. Matter* **23** 374104
Loïodice I, Staub J, Setty T G, Nguyen N P, Paoletti A and Tran P T 2005 Ase1p organizes antiparallel microtubule arrays during interphase and mitosis in fission yeast *Mol. Biol. Cell* **16** 1756–68
Mollinari C, Kleman J P, Jiang W, Schoehn G, Hunter T and Margolis R L 2002 PRC1 is a microtubule binding and bundling protein essential to maintain the mitotic spindle midzone *J. Cell Biol.* **157** 1175–86
Peloquin J, Komarova Y and Borisy G 2005 Conjugation of fluorophores to tubulin *Nature Methods* **2** 299–303
Pierce D W and Vale R D 1998 Assaying processive movement of kinesin by fluorescence microscopy *Methods Enzymol.* **298** 154–71
Ross J L, Shuman H, Holzbaur E L and Goldman Y E 2008 Kinesin and dynein-dynactin at intersecting microtubules: motor density affects dynein function *Biophys. J.* **94** 3115–25
Sanchez T, Welch D, Nicastro D and Dogic Z 2011 Cilia-like beating of active microtubule bundles *Science* **333** 456–9
Schaller V, Weber C, Semmrich C, Frey E and Bausch A R 2010 Polar patterns of driven filaments *Nature* **467** 73–7
Schuyler S C, Liu J Y and Pellman D 2003 The molecular function of Ase1p: evidence for a MAP-dependent midzone-specific spindle matrix. Microtubule-associated proteins *J. Cell Biol.* **160** 517–28
Smertenko A P, Chang H Y, Wagner V, Kaloriti D, Fenyk S, Sonobe S, Lloyd C, Hauser M T and Hussey P J 2004 The Arabidopsis microtubule-associated protein AtMAP65-1: molecular analysis of its microtubule bundling activity *Plant Cell* **16** 2035–47
Subramanian R, Wilson-Kubalek E M, Arthur C P, Bick M J, Campbell E A, Darst S A, Milligan R A and Kapoor T M 2010 Insights into antiparallel microtubule crosslinking by PRC1, a conserved nonmotor microtubule binding protein *Cell* **142** 433–43
Sumino Y, Nagai K H, Shitaka Y, Tanaka D, Yoshikawa K, Chaté H and Oiwa K 2012 Large-scale vortex lattice emerging from collectively moving microtubules *Nature* **483** 448–52
Svoboda K, Schmidt C F, Schnapp B J and Block S M 1993 Direct observation of kinesin stepping by optical trapping interferometry *Nature* **365** 721–7
Tulin A, McClerklin S, Huang Y and Dixit R 2012 Single-molecule analysis of the microtubule cross-linking protein MAP65–1 reveals a molecular mechanism for contact-angle-dependent microtubule bundling *Biophys. J.* **102** 802–9
Wicker-Planquart C, Stoppin-Mellet V, Blanchoin L and Vantard M 2004 Interactions of tobacco microtubule-associated protein MAP65–1b with microtubules *Plant J.: Cell Mol. Biol.* **39** 126–34
Yamashita A, Sato M, Fujita A, Yamamoto M and Toda T 2005 The roles of fission yeast ase1 in mitotic cell division, meiotic nuclear oscillation, and cytokinesis checkpoint signaling *Mol. Biol. Cell* **16** 1378–95
Zhu C, Lau E, Schwarzenbacher R, Bossy-Wetzel E and Jiang W 2006 Spatiotemporal control of spindle midzone formation by PRC1 in human cells *Proc. Natl Acad. Sci. USA* **103** 6196–201